Calculation of conformation-dependent biomolecular forces

Wonmuk Hwang[a)]
Department of Biomedical Engineering, Texas A&M University, College Station, Texas 77843, USA

(Received 21 May 2007; accepted 22 August 2007; published online 5 November 2007)

We develop a numerical scheme that calculates forces under *given* conformational states of a biomolecule by using a harmonic sampling potential. It can also be used for calculating the potential of mean force, as tested by random walks on Gaussian enthalpy barriers. Further, Brownian dynamics simulations of a finite-length freely jointed chain confirm the analytic expressions for its entropic elasticity that we derive. Our method, while generally applicable to many systems, will be particularly useful for studying the elasticity of biopolymers where various types of ensembles differ due to the finite size effect. © *2007 American Institute of Physics*. [DOI: 10.1063/1.2784557]

I. INTRODUCTION

Recent developments in single molecule manipulation methods have revealed mechanical force as a key mediator in biomolecular processes.[1] Unlike free energy, an equilibrium concept, force is a directly measurable and manipulable quantity that applies also to nonequilibrium processes. In particular, motor proteins and biopolymers[2] are widely studied by, e.g., optical traps[3] or atomic force microscopy (AFM).[4]

A challenge in computational studies of these molecular mechanical phenomena is calculating the force itself as a function of molecular conformations. In the case of biopolymers, a harmonic sampling potential $\kappa/2(\mathbf{r}-\mathbf{r}_0)^2$ ($\mathbf{r}_0$, center of the potential) can be applied to one end of the polymer ($\mathbf{r}$) while the other end is fixed at the origin. Ensemble averaging (denoted $\langle\cdot\rangle$) gives the force exerted by the polymer $\kappa\langle\mathbf{r}-\mathbf{r}_0\rangle$ at $\langle\mathbf{r}\rangle$, much like optical trap or AFM experiments. However, the average position $\langle\mathbf{r}\rangle$ is not known *a priori*, and it is difficult to calculate the force generated at a *given* position of interest. Such a question is more important when considering molecular motors, where there are force generating substeps with well-defined conformational states.[5,6]

In general, thermodynamics of finite systems differ from those of macroscopic systems.[7,8] For example, *fixed-conformation* and *fixed-force* ensembles differ, where the latter is easier to handle as force is simply a Lagrange multiplier in the Hamiltonian.[9] Well-known polymer models such as freely jointed chain (FJC) or wormlike chain thus work with fixed-force ensembles.[10,11] In principle, it is possible to get the force (which is the free energy gradient) along the reaction coordinate from free energy simulations. An example is the blue moon ensemble.[12] However, the method becomes tricky to implement for complex structures as it requires not only a rigid constraint fixing the reaction coordinate to a particular value but other quantities have also to be calculated, such as determinants of coordinate transformation matrices and their derivatives. More recently, the umbrella integration[13] uses a harmonic sampling potential that allows local fluctuations. The conformational distribution is assumed to be Gaussian and the force along the reaction coordinate can be measured as a weighted average over the entire integration interval, similar to the weighted-histogram analysis method.[14] While umbrella integration is shown to perform better in free energy calculations than the widely used umbrella sampling,[15] as in other free energy simulation methods, the focus is on the potential of mean force (free energy profile *along* the reaction coordinate), not mechanical force, which does not necessarily align with the reaction coordinate unless well chosen. Development in single molecule experiments calls for a more direct means of calculating forces in a conformation-dependent manner.

Here, we develop a fluctuation analysis method that perturbatively calculates free energy gradients *at* the point of interest. It locally uses a harmonic sampling potential without any need for overlapping distributions. Only up to second moments of fluctuations are required for calculation, which are easy to measure from the coordinate trajectory without any special manipulations. Two examples, random walk over Gaussian enthalpy barrier and entropic elasticity of a finite-length FJC, demonstrate the method. The relation between positional fluctuations and free energy gradients that we find also have implications in optical trap or AFM experiments where the probes are essentially harmonic.

II. THEORY

First consider a one-dimensional (1D) system with the free energy $F(x)$. With a harmonic sampling potential $F_S(x)=\kappa/2(x-x_0)^2$, the net Hamiltonian is $\mathcal{H}(x)=F(x)+F_S(x)+F_1$, where $F_1=F_1(\kappa,x_0)$ is a constant free energy shift caused by introducing the sampling potential.[15] For large enough κ, the system is localized near x_0, which can be expanded by $\delta x=x-x_0$,

$$\mathcal{H}=F(x_0)+F_1+F_x\delta x+\tfrac{1}{2}(\kappa+F_{xx})\delta x^2+\mathcal{O}(\delta x^3), \qquad (1)$$

where $F_x\equiv dF/dx|_{x_0}$, etc. The corresponding Boltzmann factor, $e^{-\beta\mathcal{H}}$ ($\beta=(k_BT)^{-1}$, k_B, Boltzmann constant; T, temperature) is a Gaussian, which yields

a)Electronic mail: hwm@tamu.edu

$$\langle \delta x \rangle = -\frac{F_x}{\kappa + F_{xx}}, \quad \mathrm{var}(\delta x) = \frac{k_B T}{\kappa + F_{xx}}. \tag{2}$$

We thus get the gradients

$$F_x = -\frac{k_B T}{\mathrm{var}(\delta x)} \langle \delta x \rangle, \quad F_{xx} = \frac{k_B T}{\mathrm{var}(\delta x)} - \kappa. \tag{3}$$

Note that these are evaluated at the prescribed position x_0, not $\langle x \rangle$, and that the expressions are local, without any need to consider the behavior at other points. The force, $-F_x$, does not explicitly involve the stiffness κ, as a manifestation of the equipartition theorem.[16] Higher order terms involve $\langle \delta x^3 \rangle$, but gradients should be evaluated numerically, which we do not pursue further here.

In higher dimensions, expansion of $F(\mathbf{r})$ involves cross-dimensional terms. Ignoring constants,

$$\mathcal{H} \simeq \sum_i (A_i \delta r_i^2 + F_i \delta r_i) + \sum_{\{i,j\}} F_{ij} \delta r_i \delta r_j,$$
$$A_i \equiv \tfrac{1}{2}(\kappa_i + F_{ii}), \quad \delta r_i = r_i - r_{0i}. \tag{4}$$

Here, κ_i is the stiffness of $F_S(\mathbf{r})$ in the i direction and $\{i,j\}$ denotes all permutations of $i \neq j$. In effect, $\mathcal{H}$ is the deformation of the steep parabolic surface $F_S(\mathbf{r})$ by the more slowly varying $F(\mathbf{r})$. The corresponding expressions for the gradients are (Appendix A)

$$F_i \simeq -\frac{k_B T}{\mathrm{var}(\delta r_i)} \langle \delta r_i \rangle - \sum_{j \neq i} F_{ij} \langle \delta r_j \rangle, \tag{5}$$

$$F_{ii} \simeq \frac{k_B T}{\mathrm{var}(\delta r_i)} - \kappa_i, \tag{6}$$

$$F_{ij} \simeq -k_B T \frac{\mathrm{cov}(\delta r_i, \delta r_j)}{\mathrm{var}(\delta r_i)\mathrm{var}(\delta r_j)}. \tag{7}$$

Here, the second term on the right hand side in Eq. (5) is a correction to the 1D expression, Eq. (3).

III. RANDOM WALK ON GAUSSIAN ENTHALPY BARRIER

Equations (3) and (5)–(7) are the central results of this approach. To test, we consider a random walk in a field described by the Langevin equation. In 1D,

$$m\frac{d^2x}{dt^2} = -\zeta\frac{dx}{dt} + f(x) + \xi(t) - \kappa(x - x_0). \tag{8}$$

Here, m is the mass, $\zeta = 6\pi\eta x^\star$ (η, solvent viscosity; $x^\star$, hydrodynamic radius of the walker) is the damping coefficient, $f(x) = -(d/dx)F(x)$ is the external field to be tested, and $\xi(t)$ is the random force that satisfies the fluctuation-dissipation theorem.[17] For numerical implementation, we dedimensionalize Eq. (8) as follows. The units of length and time are chosen as the hydrodynamic radius $x^\star$ and the diffusion time over $x^\star$, $t^\star = x^{\star 2}\zeta/(k_B T^\star)$ ($T^\star = 300$ K). Other units used are $\epsilon^\star = k_B T^\star$ (energy), $f^\star = \zeta x^\star / t^\star$ (force), and $m^\star = \zeta t^\star$ (mass). Setting $x = x^\star x'$, $t = t^\star t'$, $f = f^\star f'$, $\xi = f^\star \xi'$, $\kappa = f^\star \kappa' / x^\star$, $T = T^\star T'$, and $m = m^\star m'$, the dimensionless form of Eq. (8) is

$$m'\frac{d^2x'}{dt'^2} = -\frac{dx'}{dt'} + f' + \xi' - \kappa'(x' - x_0'). \tag{9}$$

For numerical implementation of the random force, from $\langle \xi(t_1)\xi(t_2) \rangle = 2\zeta k_B T \delta(t_1 - t_2)$, at each integration step, ξ' is a Gaussian random number with variance $2T'/\delta t$, where δt is the dimensionless integration time step.

To get a physical feel for the dedimensionalization, we take the example of the well-studied globular protein lysozyme in water, with $x^\star = 2.0$ nm (Ref. 18) and $m = 14.4$ kDa ($= 2.39 \times 10^{-23}$ kg). This sets $\zeta = 3.4 \times 10^{-11}$ kg/s, $t^\star = 33$ ns, $f^\star = 2.1$ pN, and $m^\star = 1.1 \times 10^{-18}$ kg. The dimensionless mass is then $m' = 2.2 \times 10^{-5}$, so the inertia term is usually dropped. However, for numerical efficiency, we keep it and set $m' = 1$ to implement the stochastic velocity Verlet algorithm, a procedure known to allow a larger time step δt than the case with $m' = 0$.[19,20] For notational simplicity, below we drop $'$ from dimensionless variables.

In the 1D case, it is relatively straightforward to construct the potential of mean force by integrating gradients. The interval of interest is divided into windows of size Δ, and sampling is performed in each window with the center of the sampling potential at the nth window given by $x_0^{(n)} = x_0^{(0)} + n\Delta$ ($n = 0, 1, 2, \ldots$). Knowledge of the second-order gradient $F_{xx}^{(n)}$ at $x_0^{(n)}$ enhances the accuracy of integration, where the iteration formula is

$$F(x_0^{(n+1)}) - F(x_0^{(n)}) = \frac{\Delta}{2}(F_x^{(n)} + F_x^{(n+1)}) + \left(\frac{\Delta}{2}\right)^2 \frac{F_{xx}^{(n)} - F_{xx}^{(n+1)}}{2}. \tag{10}$$

Note that no additional binning nor weighted averaging is necessary, unlike other free energy simulation methods based on umbrella sampling.[13,15]

We test a Gaussian potential barrier, $F(x) = 10\exp(-x^2/2)$. This example is motivated by the general problem of transition states in protein-protein interactions, such as in enzyme-ligand binding kinetics.[21] The height of the barrier represents a typical value in dimensionful terms, $10k_B T^\star$. The simulation was run in the interval $x = [-3, 3]$, with $\Delta = 0.2$, $\delta t = 0.005$, and $T = 1$. For each window, moments of δx were calculated during 2×10^6 steps, with coordinates saved every 10 steps. Equations (3) and (10) were then used to calculate F_{xx}, F_x, and F [Figs. 1(a)–1(c)]. For $\kappa > 10$, the calculated F_x or F agree reasonably well with analytic expressions. A longer time average is required for a more accurate estimation of F_{xx}. Although in principle a larger κ would lead to a better second-order approximation in Eq. (1), finite simulation time and noninfinitesimal δt cause the moments noisier for larger κ. In particular, F_{xx} is the most affected as it involves the difference between two large numbers, $(\mathrm{var}(\delta x))^{-1}$ and κ. When $\kappa = 200$, finite difference of F_x actually gives a smoother profile for F_{xx} than that from Eq. (3) [Fig. 1(b)]. However, finite difference may become inapplicable at higher dimensions (see below) or for wide-apart sampling points.

Positional distribution of the walker for runs with $x_0 = 0$ elucidates the effect of the stiffness of the sampling potential

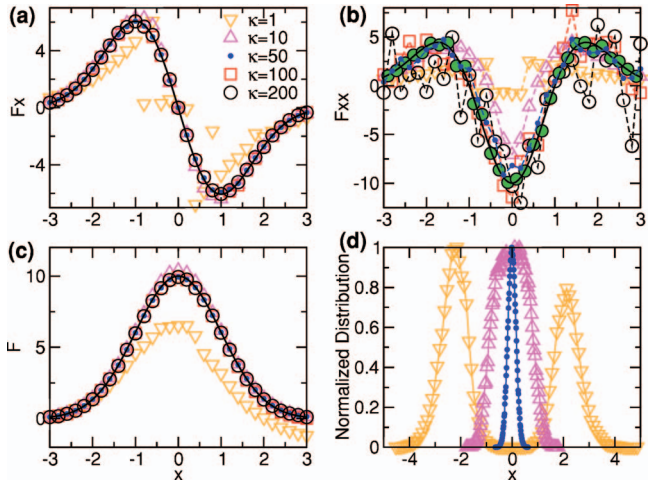

FIG. 1. (Color) 1D random walk on a Gaussian potential barrier, $F(x)=10\exp(-x^2/2)$. Solid lines in (a)–(c): from analytic expressions. Filled green circles in (b): finite differences of F_x for $\kappa=200$ in (a). (d) Peak-normalized positional distribution in the case $x_0=0$, with $\kappa=1$, 10, and 50. There are two peaks when $\kappa=1$.

[Fig. 1(d)]. For $\kappa=1$, the walker cannot stay at the peak of the barrier, so the distribution is bimodal around $x=\pm 2$. When $\kappa=10$, $\kappa+F_{xx}=0$ at the peak, so that the sampling potential locally "cancels" the barrier, rendering a broad, *non-Gaussian* distribution. The distribution becomes narrower as κ grows beyond 10. In the case of the widely used umbrella sampling, such cancellation is a desired condition; thus κ has to be adjusted window by window for maximal overlap of distributions between neighboring windows. In our approach, such a condition is not necessary, and the only practical limit in using large κ is the numerical noise.

We next use a two-dimensional (2D) asymmetric Gaussian barrier $F(\mathbf{r})=10\exp\{-\frac{1}{2}(x^2+4y^2)\}$ to test Eqs. (5)–(7). Simulation conditions were similar to the 1D case, with $\kappa_x=\kappa_y=\kappa$, and 10^7 simulation steps at each sampling point for better statistics. Sampling points were chosen along the x or y axes, or along the line $x=y$. The results were again found to agree reasonably well with analytic expressions, and we focus only on the correction term in Eq. (5) that is absent in the 1D case. The term has little contribution along the x or y axes, where the coordinate axes are principal (data not shown; see also Sec. IV). Along $x=y$, however, it can be significant, especially for small κ (Fig. 2). In this case, the force does not align with the reaction coordinate; finite differences based on free energy simulations along $x=y$ would only yield the projection of forces. Our approach reports the full force vector, thus does not require a careful choice of the reaction coordinate as most free energy simulation methods do.

IV. ENTROPIC ELASTICITY OF FINITE-LENGTH FJC

The Gaussian barriers above form the enthalpy term in the free energy. To test our approach for probing the entropic contribution, we consider a FJC that has N bonds of length b each.[11] Its free energy is purely entropic, and an analytic expression is available for $N\to\infty$. However, the finite N case does not seem to have been previously addressed in detail,

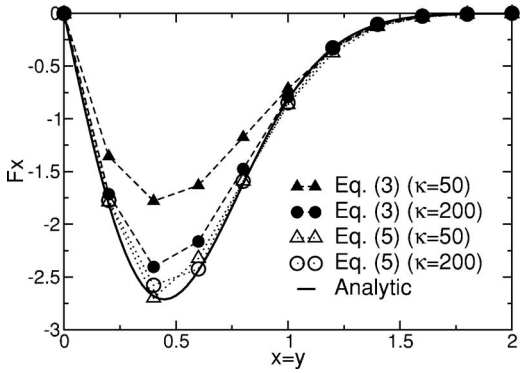

FIG. 2. Profile of F_x along the line $x=y$ for a 2D asymmetric Gaussian barrier. Data marked by "Eq. (3)" are evaluated without the correction term in Eq. (5), as in the 1D case.

although a case in the context of coarse graining[22] and other types of discrete semiflexible polymers have been theoretically considered.[9]

We performed Brownian dynamics simulations of FJC using a beads-on-a-chain model. The equation of motion for each bead is a three-dimensional (3D) version of Eq. (9) plus a term describing bond connectivity. Sampling was performed by fixing the first bead at the origin and applying the sampling potential on the last bead. We used $\delta t=0.002$ and 10^7 simulation steps at each sampling point, which gave sufficient statistics. To impose a nearly constant bond length b, we modified the finitely extensible nonlinear elastic (FENE) spring model[19] where the bonded force on the bead $(i+1)$ from the bead i is given by

$$\mathbf{f}_F=\kappa_F\frac{b(1-d/b)}{\epsilon^2-(1-d/b)^2}\frac{\mathbf{d}}{d}, \tag{11}$$

where $\mathbf{d}=\mathbf{r}_{i+1}-\mathbf{r}_i$ is the distance vector between beads i and $i+1$, $\kappa_F(=400)$ is the spring constant, and $\epsilon(=0.2)$ is the maximum strain allowed on the bond. While the regular flexible FENE chain is known to be different from the freely jointed Kramers chain with rigid bonds,[23] the bond described by Eq. (11) is quite stiff, and the above choice of parameters resulted in only small bond elongation even at the maximum extension tested (99%). Rather, b, κ, and T had greater effects, which reveal the behavior of the system better.

Two types of ensembles were considered [Fig. 3(a)]. In the x-constrained ensemble (x-CE), $F_S(\mathbf{r})=(\kappa/2)\delta x^2$, so that the last bead fluctuates freely on the yz plane, while in the xyz-constrained ensemble (xyz-CE), $F_S(\mathbf{r})=(\kappa/2)(\delta x^2+y^2+z^2)$, that constrains the bead on the x axis.

The x-CE with a finite N can be described analytically. For $N=1$, the probability distribution $P_1(x)dx$ for the x coordinate of the moving end is proportional to the area of the strip on a shell of radius b within $(x,x+dx)$, which is $2\pi b dx$. Since $P_1(x)\sim e^{S(x)/k_B}$ [$S(x)$, entropy of the system], the free energy $F=-k_BT\ln(P_1)$, and the resultant force $f=-\partial_x F=0$. Since P_1 is constant, $P_{N>1}$ can be regarded as an N-step random walk in the x direction where each step has a uniform probability distribution in the range $[-b,+b]$. For $N=2$,

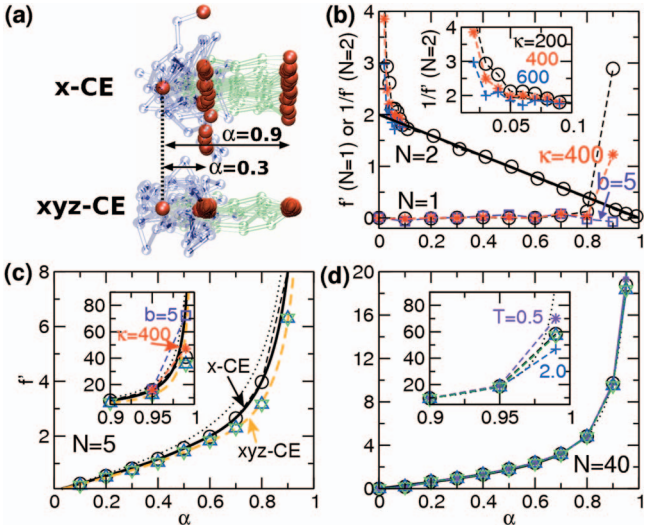

FIG. 3. (Color) Force-extension relation of FJC. (a) Example snapshots of the two ensembles overlaid at two extensions. [(b)–(d)] $f'=-fb/T$ vs $\alpha=x/Nb$. Thick solid: Eqs. (13) and (14). In (c) and (d), black dotted: $\alpha=\coth(f')-1/f'$, for $N\to\infty$ (Ref. 11). In (c), thick orange dashed: analytic result for *xyz*-CE with $N=5$ [Eqs. (42) and (43) in Ref. 22]. Open circle: *x*-CE [Eq. (3)]. Blue up and green down triangles: *xyz*-CE with and without the correction term in Eq. (5), which nearly coincide due to the radial symmetry (cf. Fig. 2). Unless otherwise noted on the graph, $b=1$, $\kappa=200$, and $T=1.0$. Insets: magnification for small α (b) and α near 1 [(c) and (d)].

$$P_2(x)\sim\int_{-b}^{+b}dx_1\int_{-b}^{+b}dx_2\delta(x_1+x_2-x)=2b-|x|. \tag{12}$$

For $x>0$, the corresponding force is

$$f(x)=-\frac{k_BT}{2b-x}\quad(N=2). \tag{13}$$

For general N, the force is (see Appendix B)

$$f(x)=-k_BT\frac{\int_0^\infty dqq\,\sin(qx)\{\sin(qb)/q\}^N}{\int_0^\infty dq\,\cos(qx)\{\sin(qb)/q\}^N}. \tag{14}$$

The *xyz*-CE is identical to a 3D random walk with a fixed step size b. This case has been previously considered and an expression similar to Eq. (14) exists.[22,24]

Forces are measured in simulations using Eq. (3) for *x*-EC and Eq. (5) for *xyz*-CE. For $N=1$, only *x*-EC is possible, and the force stays close to 0 until $\alpha=x/Nb$ is above 0.8. Divergence for $\alpha\to1$ is due to the finite size of thermal motion compared to the residual range $(1-\alpha)b$, so that any transverse fluctuation results in reduction of the x position when $\alpha\to1$. This effect can be reduced by increasing either b or κ for stronger confinement [Fig. 3(b)]. The divergence is not a discrete time effect, since using a smaller δt did not mitigate it.

For $N=2$ (*x*-CE), $1/f'$ vs α is a straight line that intersects 2 [f', rescaled force; Fig. 3(b)]. f' vanishes as $\alpha\to0$ as $\lim_{x\to0^\pm}f'=\pm1/2$ [Eq. (13)]. Using higher values of κ extends the straight line for smaller α, as the last bead passes through $x=0$ less frequently [Fig. 3(b), inset]. For $N=5$, we consider both *x*-CE and *xyz*-CE that generate less forces than the $N\to\infty$ case. The weakest is *xyz*-CE due to the additional confinement [Fig. 3(c)]. Both cases agree well with analytic expressions except at high extensions where $F(\mathbf{r})$ varies as fast as $F_S(\mathbf{r})$, weakening the approximation used. For $N=40$, all cases become nearly indistinguishable [Fig. 3(d)], consistent with the central limit theorem.[16] In the case of *x*-CE, discrepancies near $\alpha\to1$ are shown to decrease with larger b or κ, as for $N=1$, or with lower T [Figs. 3(c) and 3(d), insets]. Thus, varying κ or T in simulations would be a self-consistent way of checking the calculation.

V. CONCLUSION

Our formalism can be generalized, e.g., to other coordinate systems, or by making the spring constant of the sampling potential as a tensor of rank 2. However, the approach based on the Cartesian coordinate system allows simple analytic expressions [Eqs. (3) and (5)–(7)] that would be useful for many different situations. As demonstrated in Sec. III, it can also be used for calculating the potential of mean force. However, for calculating mechanical forces, defining a reaction coordinate is not necessary since only the points of interest need to be considered. Other than examples considered here, we used this approach to calculate the magnitude of kinesin's power stroke.[6]

The present approach can further be used for studying the elasticity of semiflexible polymers that are essential for cytoskeletal dynamics. As observed in FJC, the finite size effect can significantly alter the response of the system. Simulations in this regard would have direct relevance to single molecule experiments where a full range of extensions can now be probed for cases when the persistence length is comparable to the chain length.[25] While the present analysis is applicable mainly to simulations, a similar approach has been taken in a recent AFM study that analyzed thermal fluctuations of the AFM cantilever to calculate the stiffness of selectins.[26] Within the extension range tested, they observed a linear force-extension behavior; thus a simple 1D analysis was effective. For a more complex response, the formalism developed here would be more illuminating.

ACKNOWLEDGMENTS

This work was partially funded by the NIH Grant Nos. 1 R21 NS058604-01 and GM076689. I would like to thank R. D. Kamm for helpful discussions.

APPENDIX A: DERIVATION OF EQUATIONS (5)–(7)

For notational convenience, we choose the coordinate origin at the center of $F_S(\mathbf{r})$, to change δr_i to r_i, and absorb the inverse temperature into the coefficients in Eq. (4), which yields

$$\beta\mathcal{H}\simeq\sum_i(A_ir_i^2+B_ir_i)+\sum_{\{i,j\}}C_{ij}r_ir_j$$
$$A_i\equiv\frac{\beta}{2}(\kappa_i+F_{ii}),\quad B_i\equiv\beta F_i,\quad C_{ij}\equiv\beta F_{ij}. \tag{A1}$$

Note that A_i has been redefined. Since $A_i\gg C_{ij}$ and only small values of $\{r_i\}$ are relevant, we expand the Boltzmann factor as follows:

$$e^{-\beta\mathcal{H}} \sim \left(1 - \sum_{\{i,j\}} C_{ij} r_i r_j\right) e^{-\Sigma_l A_l (r_l - \lambda_l)^2}, \quad \lambda_l \equiv -\frac{B_l}{2A_l}. \tag{A2}$$

The partition function is

$$Z \simeq \int d\mathbf{r}\left(1 - \sum_{\{i,j\}} C_{ij} r_i r_j\right) e^{-H_0} = Z_0\left(1 - \sum_{\{i,j\}} C_{ij}\lambda_i\lambda_j\right),$$
$$H_0 \equiv \sum_l A_l (r_l - \lambda_l)^2, \quad Z_0 \equiv \prod_k \sqrt{\pi/A_k}. \tag{A3}$$

With the above, we can calculate the average

$$\langle r_i \rangle = \frac{1}{Z}\int d\mathbf{r}\left(r_i - r_i^2 \sum_{j\neq i} C_{ij} r_j - r_i \sum_{\{j,k\}}{}' C_{jk} r_j r_k\right) e^{-H_0}, \tag{A4}$$

where the last summation is on all permutations of j and k different from i. Note that

$$\int d\mathbf{r} r_j e^{-H_0} = \lambda_j Z_0,$$
$$\int d\mathbf{r} r_i^2 e^{-H_0} = Z_0\left(\frac{1}{2A_i} + \lambda_i^2\right). \tag{A5}$$

Using $\lambda_i \propto A_i^{-1}$, and keeping terms up to the order A_i^{-2}, we can drop the third term on the right hand side of Eq. (A4), and get

$$\langle r_i \rangle \simeq \lambda_i - \frac{1}{2A_i}\sum_{j\neq i} C_{ij}\lambda_j. \tag{A6}$$

Similarly, for variance and covariance, keeping terms up to A_i^{-2},

$$\mathrm{var}(r_i) \simeq \frac{1}{2A_i}, \quad \mathrm{cov}(r_i, r_j) \simeq -\frac{C_{ij}}{4A_iA_j}. \tag{A7}$$

The second order term in $\mathrm{var}(r_i)$ is 0. Also note that the C_{ij} term in Eq. (A3) has no contribution to the moments calculated above, so effectively $Z \simeq Z_0$ to this order. The covariance is smaller than the variance since the spring constant for the sampling potential, $\{\kappa_i\}$ as a tensor, is diagonal in our formalism. Combining Eqs. (A6) and (A7), and restoring the notation $r_i \to \delta r_i$, yields Eqs. (5)–(7).

APPENDIX B: DERIVATION OF EQUATION (14)

Considering Eq. (12),

$$P_N(x) \sim \int_{-b}^{+b} dx_1 \cdots dx_N \delta\left(\sum_{n=1}^{N} x_n - x\right)$$
$$= \int_{-b}^{+b} dx_1 \cdots dx_N \int_{-\infty}^{+\infty} \frac{dq}{2\pi} e^{iq(\Sigma_n x_n - x)}. \tag{B1}$$

Using $\int_{-b}^{+b} dx_n \exp(iqx_n) = 2\sin(qb)/q$,

$$P_N(x) \sim 2^N \int_{-\infty}^{+\infty} dq e^{-iqx}\{\sin(qb)/q\}^N$$
$$= 2^N \int_0^{\infty} dq (e^{-iqx} + e^{iqx})\{\sin(qb)/q\}^N$$
$$= 2^{N+1} \int_0^{\infty} dq \cos(qx)\{\sin(qb)/q\}^N. \tag{B2}$$

Now, $f = k_B T (d/dx) \ln(P_N)$ yields Eq. (14).

[1] C. Bustamante, Y. R. Chemla, N. R. Forde, and D. Izhaky, Annu. Rev. Biochem. **73**, 705 (2004).
[2] J. Howard, *Mechanics of Motor Proteins and the Cytoskeleton* (Sinauer, Sunderland, MA, 2001).
[3] E. A. Abbondanzieri, W. J. Greenleaf, J. W. Shaevitz, R. Landick, and S. M. Block, Nature (London) **438**, 460 (2006).
[4] H. Li, W. A. Linke, A. F. Oberhauser, M. Carrion-Vazquez, J. G. Kerkvliet, H. Lu, P. E. Marszalek, and J. M. Fernandez, Nature (London) **418**, 998 (2002).
[5] *Molecular Motors*, edited by M. Schliwa (Wiley-VCH, New York, 2003).
[6] W. Hwang, M. J. Lang, and M. Karplus, Stucture, "Force Generation in Kinesin Hinges on Cover-Neck Bundle Formation" (to be published).
[7] T. L. Hill, *Thermodynamics of Small Systems* (Dover, New York, 2002).
[8] C. Bustamante, J. Liphardt, and F. Ritort, Phys. Today **58**(7), 43 (2005).
[9] L. Livadaru, R. R. Netz, and H. J. Kreuzer, Macromolecules **36**, 3732 (2003).
[10] J. F. Marko and E. D. Siggia, Macromolecules **28**, 8759 (1995).
[11] M. Fixman and J. Kovac, J. Chem. Phys. **58**, 1564 (1973).
[12] E. A. Carter, G. Ciccotti, J. T. Hynes, and R. Kapral, Chem. Phys. Lett. **156**, 472 (1989).
[13] J. Kästner and W. Thiel, J. Chem. Phys. **123**, 144104 (2005).
[14] A. M. Ferrenberg and R. H. Swendsen, Phys. Rev. Lett. **63**, 1195 (1989).
[15] B. Roux, Comput. Phys. Commun. **91**, 275 (1995).
[16] F. Reif, *Fundamentals of Statistical and Thermal Physics* (McGraw-Hill, Tokyo, Japan, 1965).
[17] N. G. Van Kampen, *Stochastic Processes in Physics and Chemistry* (Elsevier, Netherlands, 1992).
[18] J. G. de la Torre, M. L. Huertas, and B. Carrasco, Biophys. J. **78**, 719 (2000).
[19] R. Rzehak, A. Arend, D. Kienle, and W. Zimmermann, *Polymer and Cell Dynamics*, edited by W. Alt, M. Chaplain, M. Griebel, and J. Lenz (Birkhäuser, Basel, Switzerland, 2003), pp. 49–68.
[20] G. Ciccotti and G. Kalibaeva, Philos. Trans. R. Soc. London, Ser. A **362**, 1583 (2004).
[21] J. Kottalam and D. A. Case, J. Am. Chem. Soc. **110**, 7690 (1988).
[22] P. T. Underhill and P. S. Doyle, J. Rheol. **49**, 963 (2005).
[23] A. V. Lyulin, D. B. Adolf, and G. R. Davies, J. Chem. Phys. **111**, 758 (1999).
[24] L. R. G. Treloar, *The Physics of Rubber Elasticity* (Clarendon, Oxford, UK, 1975).
[25] A. S. Khalil, J. M. Ferrer, R. R. Brau, S. T. Kottmann, C. J. Noren, M. J. Lang, and A. M. Belcher, Proc. Natl. Acad. Sci. U.S.A. **104**, 4892 (2007).
[26] B. T. Marshall, K. K. Sarangapani, J. Wu, M. B. Lawrence, R. P. McEver, and C. Zhu, Biophys. J. **90**, 681 (2006).